VNU Journal of Science: Mathematics – Physics, Vol. 36, No. 4 (2020) 35-45

VNU Journal of Science: Mathematics - Physics

Journal homepage: https://js.vnu.edu.vn/MaP

Original Article

Investigating Scalar Unparticle Production at $\mu^+\mu^-$ Collisions with Polarized $\mu^+\mu^-$ Beams in Unparticle Physics

Le Mai Dung*, Dao Thi Le Thuy

Department of Physics, Hanoi National University of Education, 136 Xuan Thuy, Cau Giay, Hanoi, Vietnam

Received 16 March 2020
Revised 10 April 2020; Accepted 12 August 2020

Abstract: Scalar unparticle production in the process $\mu^+\mu^- \to ZU$ is studied from unparticle physics perspective. We have calculated and evaluated the cross sections for muon and Z boson exchange when the $\mu^+\mu^-$ beams are initially polarized. Numerical calculations show that the cross section of $\mu^+\mu^-$ collisions depends strongly on the polarized condition of the initial beams and the collision energy $\sqrt{s}$. The results are plotted in the energy reach available at the present accelerators and the future high energy frontier muon colliders as shown in the scheme by Muon Accelerator Program (MAP) and other different colliders.

Keywords: Scalar unparticle production, unparticle physics, $\mu^+\mu^-$ collisions, muon colliders.

1. Introduction

At low energy, the Standard Model (SM) describes our real world successfully in terms of particles. In our common-sense notion, particles have definite mass and carry energy and momentum in a relativistic dispersion relation. In a scale invariant world, however, particles must have zero mass in order to satisfy rescaling in a scale transformation. That is contrary to our world wherein there are plenty of particles with non-zero mass. Hence, a scale invariant sector exists then it has to be conserved beyond the SM at TeV to multi-TeV scale. Based on the vector-like non-abelian gauge theory with a large number of massless fermions studied by Banks and Zaks [1], Georgi has observed the nontrivial scale invariance sector and termed as "unparticle" [2]. Recently, experiments searching for unparticle products

*Corresponding author.
Email address: lmaidung@gmail.com

https//doi.org/ 10.25073/2588-1124/vnumap.4489

have been performed by using Compact Muon Solenoid (CMS) detector at Large Hadron Collider (LHC) or e^+e^- colliders [3-5]. However, next generation energy-frontier particle physics facilities must provide an energy reach beyond that of the LHC, with the ability of discovering new physics and still be within reasonable budget [6-8]. The extension of e^+e^- colliders to multi-TeV energy scale is performance-limited by beamstrahlung and cost-constrained, leading to the introduction of high energy muon colliders [9].

Unparticle physics. According to Georgi [2], the very high energy theory contains the SM field and BZ (for Banks-Zaks) fields with a nontrivial infrared fixed point. The operators O_{BZ} made of BZ fields interacting with the operators O_{SM} built out of SM fields through the exchange of particles with a large mass M_U, which has the generic form

$$\frac{1}{M_U^{d_{SM}+d_{BZ}-4}} O_{SM} O_{BZ} \tag{1}$$

where d_{SM} and d_{BZ} are mass dimensions of SM and BZ fields, respectively. Below the scale Λ_U, the BZ operators match onto the unparticle operators O_U due to dimensional transmutation from renormalization effects in the BZ sector [10], (1) has the following form

$$C_{O_U} \frac{\Lambda_U^{d_{BZ}-d_U}}{M_U^{d_{SM}+d_{BZ}-4}} O_{SM} O_U \tag{2}$$

where d_U is the scaling dimension of the unparticle operator O_U and the constant C_{O_U} is a coefficient function fixed by the matching condition. We may have the resulting unparticle operators with different Lorentz structures depending on the original operator O_{BZ} and the transmutation, as indicated in [2]. In this article, we will work with the scalar unparticle operator as production in $\mu^+\mu^-$ collisions which transforms under the standard model gauge group as a standard model singlet [11, 12]. Feynman rules for all unparticle operators as scalar, vector and spinor coupled to those standard model invariant operators are studied and also given explicitly in [11]. All effective interactions that satisfy the standard model gauge symmetry for the scalar unparticle operators with SM fields in [11], are given by

$$\lambda_0 \frac{1}{\Lambda_U^{d_U-1}} \overline{f} f O_U,\ \lambda_0 \frac{1}{\Lambda_U^{d_U-1}} \overline{f} i\gamma^5 f O_U,\ \lambda_0 \frac{1}{\Lambda_U^{d_U}} \overline{f}\gamma^\mu f \left(\partial_\mu O_U\right),\ \lambda_0 \frac{1}{\Lambda_U^{d_U}} G_{\alpha\beta} G^{\alpha\beta} O_U \tag{3}$$

where $G^{\alpha\beta}$ denotes the gauge field strength tensor, f represents a standard model fermion and λ_i are dimensionless effective couplings $\frac{C_{O_U^i} \Lambda_U^{d_{BZ}}}{M_U^{d_{SM}+d_{BZ}-4}}$ from the form (2) with the index i = 0, 1 or 2 corresponding to the scalar, vector and tensor unparticle operators, respectively. Here we label coupling constant λ_i with i = 0 for the effective interactions and scalar unparticle operators.

We will have Feynman rules for the scalar unparticle operators from (3) as follows

$$i\frac{\lambda_0}{\Lambda_U^{d_U-1}},\ \frac{-\lambda_0}{\Lambda_U^{d_U-1}}\gamma^5,\ \frac{\lambda_0}{\Lambda_U^{d_U}} \not{p},\ 4i\frac{\lambda_0}{\Lambda_U^{d_U}}\left(-p_1.p_2 g^{\mu\nu} + p_1^\nu p_2^\mu\right) \tag{4}$$

it can be seen that the scalar operator O_U coupled to fermion is suppressed by the mass of fermion.

Muon colliders. Let us turn back to the high energy muon colliders in which unparticle production of $\mu^+\mu^-$ collisions might be studied. Theoretically, muon and electron have the same advantage in energy but muons can be accelerated and stored in smaller rings than a hadron collider ring at the same energy reach because of negligible beamstrahlung effect. In addition, the needs of modern high energy physics (HEP) require two types of accelerator facilities, one is Higgs Factory (HF) and the other is Energy Frontier (EF) collider including e^+e^- colliders, circular e^+e^- colliders, *pp/ep* colliders and multi-TeV muon colliders. Precision measurements of masses, widths and Higgs production and new physics could be studied effectively through the muon colliders. Thus, the considered region of energy will be proposed in the Discussion section.

2. Calculation

First of all, we concentrate on the scalar unparticle production *U* of the process $\mu^+\mu^- \to ZU$ by giving the scattering amplitude *M* for each polarized $\mu^+\mu^-$ beams labeled as *LL, RR, RL, LR* in s-, t- and u-channels. Regarding the polarized conditions, the incoming beams are denoted as $\mu^+\mu^-$, each particle corresponds to the condition *L* or *R* as it says left-handed or right-handed particle. Secondly, we calculate the squared matrix elements $\left|\overline{\mathrm{M}}\right|^2$ and evaluate numerical results.

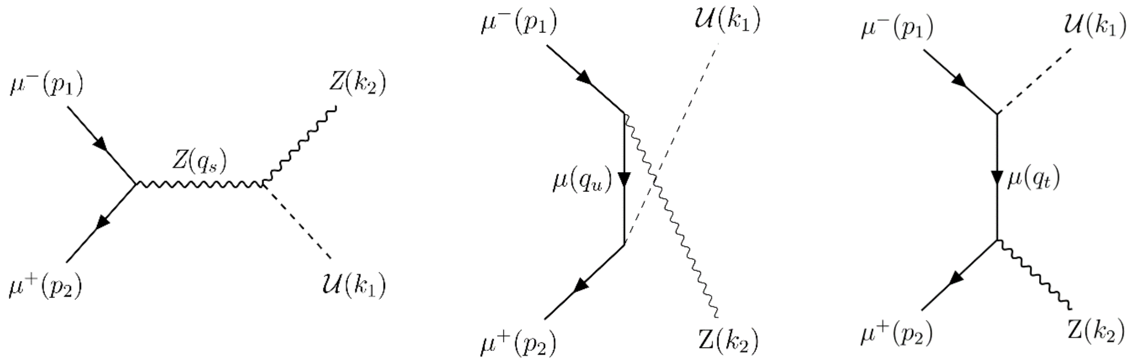

s-channel u-channel t-channel

Figure 1. The Feynman diagrams for U production through $\mu^+\mu^- \to ZU$

Applying the Feynman rules and effective interactions (3) above, we have the diagrams in Figure 1 and the scattering amplitude M_s, M_t, and M_u are below, while M_{sLR} and M_{sRL} are zero

$$\begin{aligned} M_{sLL} = &-\frac{ig\left(v_\mu + a_\mu\right)}{2c_W\left(q_s^2 - m_Z^2\right)} \frac{\lambda_0}{\Lambda_U^{d_U}} \left(\left(q_s k_2\right) g^{\alpha\nu} - q_s^\alpha k_2^\nu\right) \varepsilon_\alpha^*\left(k_2, \lambda\right)\left(g_{\nu\mu} - \frac{q_{s\nu} q_{s\mu}}{m_Z^2}\right) \\ &\times \bar{v}\left(p_2, s_2\right)\gamma^\mu\left(1-\gamma^5\right) u\left(p_1, s_1\right), \end{aligned} \quad (5)$$

$$M_{sRR} = -\frac{ig\left(v_\mu - a_\mu\right)}{2c_W\left(q_s^2 - m_Z^2\right)}\frac{\lambda_0}{\Lambda_U^{d_U}}\left(\left(q_s k_2\right)g^{\alpha\nu} - q_s^\alpha k_2^\nu\right)\varepsilon_\alpha^*\left(k_2,\lambda\right)\left(g_{\nu\mu} - \frac{q_{s\nu}q_{s\mu}}{m_Z^2}\right) \\ \times\bar{v}\left(p_2,s_2\right)\gamma^\mu\left(1+\gamma^5\right)u\left(p_1,s_1\right) \tag{6}$$

The scattering amplitudes for u-channel are

$$M_{uLL} = -\frac{ig\left(v_\mu + a_\mu\right)}{16c_W\left(q_u^2 - m_Z^2\right)}\frac{\lambda_0}{\Lambda_U^{d_U-1}}\varepsilon_\alpha^*\left(k_2,\lambda\right)\bar{v}\left(p_2,s_2\right)\left(1+\gamma^5\right)\left(1+i-\frac{i\not{k}_1}{\Lambda_U}\right) \\ \times\left(\not{q}_u + m_\mu\right)\gamma^\alpha\left(1-\gamma^5\right)u\left(p_1,s_1\right), \tag{7}$$

$$M_{uRR} = -\frac{ig\left(v_\mu - a_\mu\right)}{16c_W\left(q_u^2 - m_Z^2\right)}\frac{\lambda_0}{\Lambda_U^{d_U-1}}\varepsilon_\alpha^*\left(k_2,\lambda\right)\bar{v}\left(p_2,s_2\right)\left(1-\gamma^5\right)\left(1-i-\frac{i\not{k}_1}{\Lambda_U}\right) \\ \times\left(\not{q}_u + m_\mu\right)\gamma^\alpha\left(1+\gamma^5\right)u\left(p_1,s_1\right), \tag{8}$$

$$M_{uLR} = -\frac{ig\left(v_\mu - a_\mu\right)}{16c_W\left(q_u^2 - m_Z^2\right)}\frac{\lambda_0}{\Lambda_U^{d_U-1}}\varepsilon_\alpha^*\left(k_2,\lambda\right)\bar{v}\left(p_2,s_2\right)\left(1+\gamma^5\right)\left(1+i-\frac{i\not{k}_1}{\Lambda_U}\right) \\ \times\left(\not{q}_u + m_\mu\right)\gamma^\alpha\left(1+\gamma^5\right)u\left(p_1,s_1\right), \tag{9}$$

$$M_{uRL} = -\frac{ig\left(v_\mu + a_\mu\right)}{16c_W\left(q_u^2 - m_Z^2\right)}\frac{\lambda_0}{\Lambda_U^{d_U-1}}\varepsilon_\alpha^*\left(k_2,\lambda\right)\bar{v}\left(p_2,s_2\right)\left(1-\gamma^5\right)\left(1-i-\frac{i\not{k}_1}{\Lambda_U}\right) \\ \times\left(\not{q}_u + m_\mu\right)\gamma^\alpha\left(1-\gamma^5\right)u\left(p_1,s_1\right) \tag{10}$$

We have the scattering amplitudes for t-channel

$$M_{tLL} = -\frac{ig\left(v_\mu + a_\mu\right)}{16c_W\left(q_t^2 - m_Z^2\right)}\frac{\lambda_0}{\Lambda_U^{d_U-1}}\varepsilon_\alpha^*\left(k_2,\lambda\right)\bar{v}\left(p_2,s_2\right)\gamma^\alpha\left(1-\gamma^5\right)\left(\not{q}_t + m_\mu\right) \\ \times\left(1-i-\frac{i\not{k}_1}{\Lambda_U}\right)\left(1-\gamma^5\right)u\left(p_1,s_1\right), \tag{11}$$

$$M_{tRR} = -\frac{ig\left(v_\mu - a_\mu\right)}{16c_W\left(q_t^2 - m_Z^2\right)}\frac{\lambda_0}{\Lambda_U^{d_U-1}}\varepsilon_\alpha^*\left(k_2,\lambda\right)\bar{v}\left(p_2,s_2\right)\gamma^\alpha\left(1+\gamma^5\right)\left(\not{q}_t + m_\mu\right) \\ \times\left(1+i-\frac{i\not{k}_1}{\Lambda_U}\right)\left(1+\gamma^5\right)u\left(p_1,s_1\right), \tag{12}$$

$$M_{tLR} = -\frac{ig\left(v_\mu + a_\mu\right)}{16c_W\left(q_t^2 - m_Z^2\right)}\frac{\lambda_0}{\Lambda_U^{d_U-1}}\varepsilon_\alpha^*\left(k_2,\lambda\right)\bar{v}\left(p_2,s_2\right)\gamma^\alpha\left(1-\gamma^5\right)\left(\not{q}_t + m_\mu\right) \\ \times\left(1+i-\frac{i\not{k}_1}{\Lambda_U}\right)\left(1+\gamma^5\right)u\left(p_1,s_1\right), \tag{13}$$

$$M_{tRL} = -\frac{ig\left(v_\mu - a_\mu\right)}{16c_W\left(q_t^2 - m_Z^2\right)} \frac{\lambda_0}{\Lambda_U^{d_U-1}} \varepsilon_\alpha^*\left(k_2,\lambda\right)\bar{v}\left(p_2,s_2\right)\gamma^\alpha\left(1+\gamma^5\right)\left(\not{q}_t + m_\mu\right) \times\left(1 - i - \frac{i\not{k}_1}{\Lambda_U}\right)\left(1-\gamma^5\right)u\left(p_1,s_1\right) \tag{14}$$

where g is a coupling constant, d_U is the scaling dimension of the unparticle operator O. The squared matrix elements for s-, t- , u- channel are obtained from $\left|\overline{\mathrm{M}}\right|^2 = M^\dagger M$.

The mathematical calculation is performed in the center of mass (CM) frame of the incoming $\mu^+\mu^-$ beams, denoted by the 4-momenta p_1^μ and p_2^μ and the outgoing gauge boson Z and the scalar unparticles U with the 4-momenta k_2 and k_1, respectively. In this frame, we have

$$\begin{aligned} &p_1^\mu\left(E_1,\overrightarrow{p_1}\right),\ p_2^\mu\left(E_2,\overrightarrow{p_2}\right),\ k_1\left(E_3,\overrightarrow{k_1}\right),\ k_2\left(E_4,\overrightarrow{k_2}\right),\\ &\overrightarrow{p_1}+\overrightarrow{p_2}=\overrightarrow{k_1}+\overrightarrow{k_2}=0,\ \overrightarrow{p_1}=\vec{p},\ \overrightarrow{p_2}=-\vec{p},\ \overrightarrow{k_1}=\vec{k},\ \overrightarrow{k_2}=-\vec{k},\\ &E_1+E_2=E_3+E_4=\sqrt{s},\\ &E_1=E_2=\frac{\sqrt{s}}{2},\ E_3=\frac{m_Z^2+s}{2\sqrt{s}},\ E_4=\frac{-m_Z^2+s}{2\sqrt{s}},\\ &\left|\vec{k}\right|=\sqrt{E_3^2-m_U^2},\ \left|\vec{p}\right|=\sqrt{E_1^2-m_\mu^2} \end{aligned} \tag{15}$$

where $\sqrt{s}$ is the center-of-mass energy, $\vec{k}$ and $\vec{p}$ are momentum vectors in the initial and final state in the CM frame. After primary calculations of each squared matrix elements for each channel s, t, u, the differential cross section equation [13] is given by

$$\frac{d\sigma\left(\mu^+\mu^- \to ZU\right)}{d\cos\theta} = \frac{1}{32\pi s}\frac{\left|\vec{k}\right|}{\left|\vec{p}\right|}\left|\overline{\mathrm{M}}\right|^2 \tag{16}$$

Subsequently, we have the total cross sections σ computed by doing the numerical integration of the differential cross section over $d\cos\theta$.

3. Results and Discussion

In this section, we evaluate the existence of scalar unparticle U as final production by using the results in the previous section. We plot differential cross sections versus $\cos\theta$ of the process with each polarized $\mu^+\mu^-$ beams labeled as *LL, RR, RL, LR*. The polarized condition, left-handed or right-handed, of each particle anti-muon (μ^+) and muon (μ^-) corresponds to L or R of the label. The unparticle-related parameters we chose are as follows d_U = 1.7, λ_0 = 1 and the energy scale Λ_U = 1000 GeV [11] with $\sqrt{s}$ = 3 TeV. We fixed the value of scaling dimension d_U to evaluate the influence of polarized condition of the initial beams and the collision energy $\sqrt{s}$ on the scalar unparticle production.

At the final part of the section, we will focus on the dependence of the total cross sections on the collision energy $\sqrt{s}$, the energy is chosen in the range of $1\,\text{TeV} \le \sqrt{s} \le 10\,\text{TeV}$ with the details explained later on also in this section.

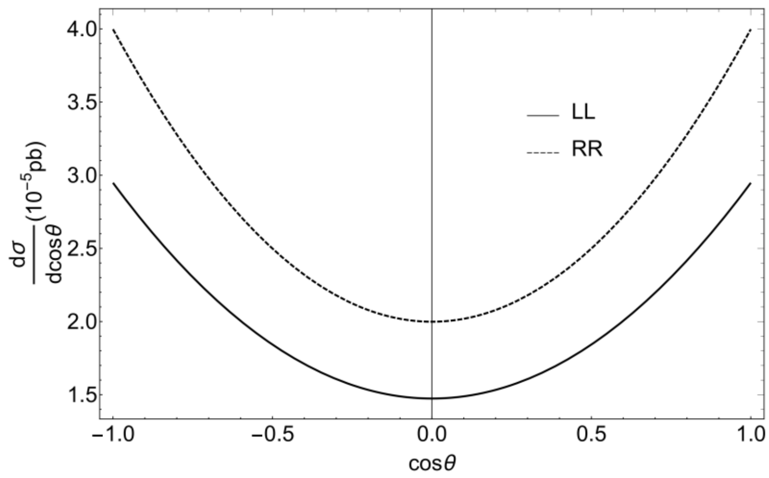

Figure 2. Differential cross sections as functions of $\cos\theta$ in s-channel with *LL* and *RR* beams at 3 TeV.

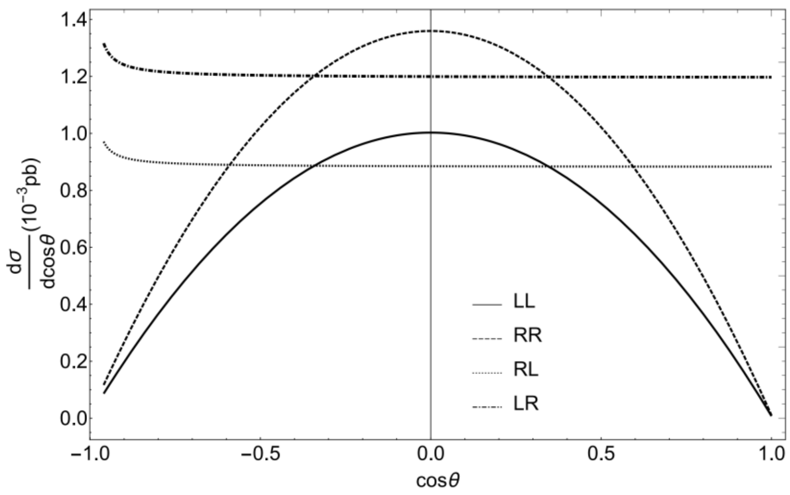

Figure 3. Differential cross sections as functions of $\cos\theta$ in u-channel with different polarized beams at 3 TeV.

We consider s-channel plotted in Figure 2 with the differential cross sections $\frac{d\sigma}{d\cos\theta}$ changing smoothly when $\cos\theta$ from -1 to 1. The maximum of *RR* cross section is at 4×10^{-5} pb when $\cos\theta$ equals to ±1 and the minimum value at 2×10^{-5} pb when the angle is of 90 degree. The same pattern is repeated for *LL*, with the value 1.3 times smaller than *RR*, meanwhile *RL* and *LR* are zero.

For u-channel in Figure 3, the differential cross sections of *RR* reaches the peak of 1.36×10^{-3} pb with $\cos\theta=0$ and the low of 0.117×10^{-3} pb when $\cos\theta=-1$ but 0.114×10^{-3} pb for $\cos\theta=1$. Meanwhile, Figure 10 shows us *RL* and *LR* differential cross sections are decreasing from the maximum of 0.902×10^{-3} and 1.22×10^{-3} pb as $\cos\theta$ raising from -1 where we have smallest value of the cross sections of the *RR* and *LL*.

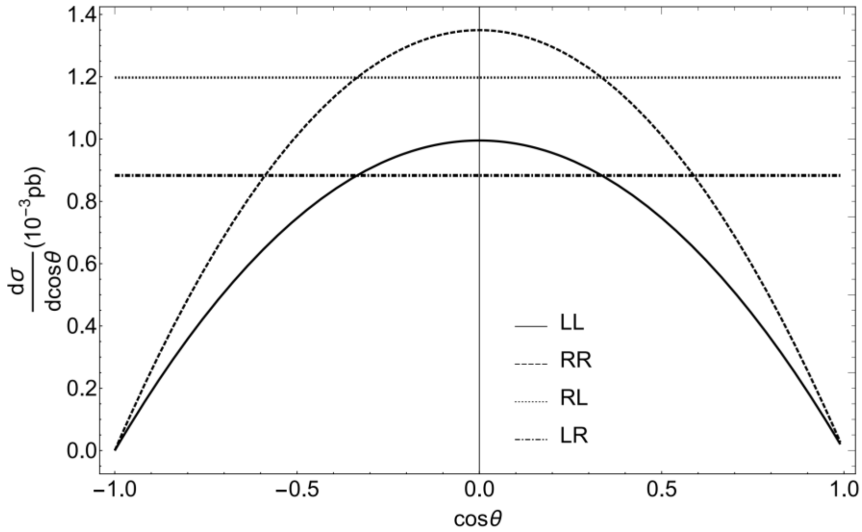

Figure 4. Differential cross sections as functions of $\cos\theta$ in t-channel with different polarized beams at 3 TeV.

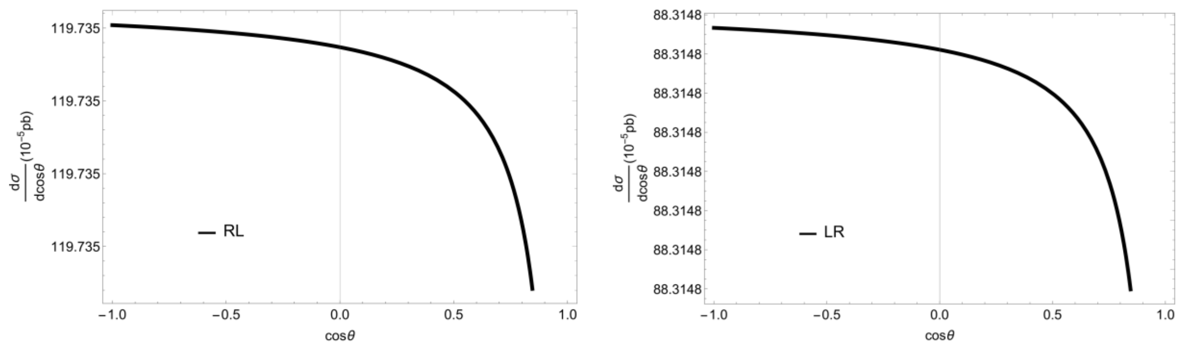

(a) RL *(b) LR*

Figure 5. Differential cross sections as functions of $\cos\theta$ for the *RL* and *LR* beams at 3 TeV.

In t-channel, Figure 4 displays that *RR* peaks at 1.35×10^{-3} when $\cos\theta$ is zero, as *RL* and *LR* (Figure 5) have limited changes at around 119.735×10^{-5} and 88.31×10^{-5} pb, respectively. On the whole, the differential cross sections of *RL* and *LR* is large enough to be not negligible over the region from -1 to 1 in Figure 5a and 5b.

Overall, the *RR* beams dominate the probability of observing unparticle in the perpendicular direction to the incoming $\mu^+\mu^-$ beams in both u- and t- channels when $\sqrt{s}=3$ TeV, while we also do not skip the *RL* and *LR* in the backward direction to the outgoing production.

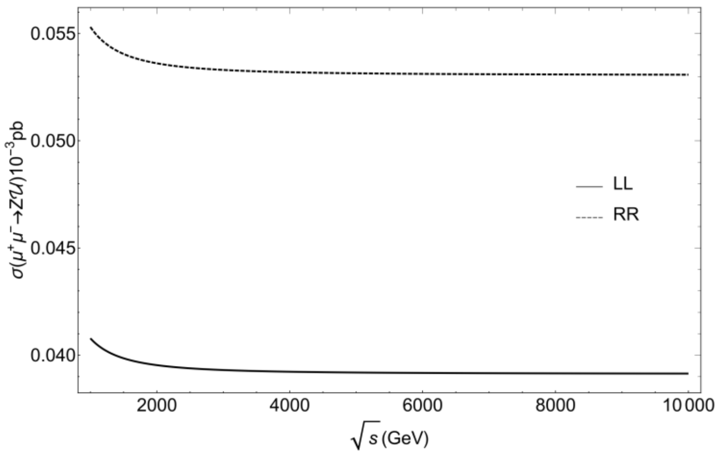

Figure 6. Total cross sections as functions of $\sqrt{s}$ for the process $\mu^+\mu^- \to ZU$ through s-channel.

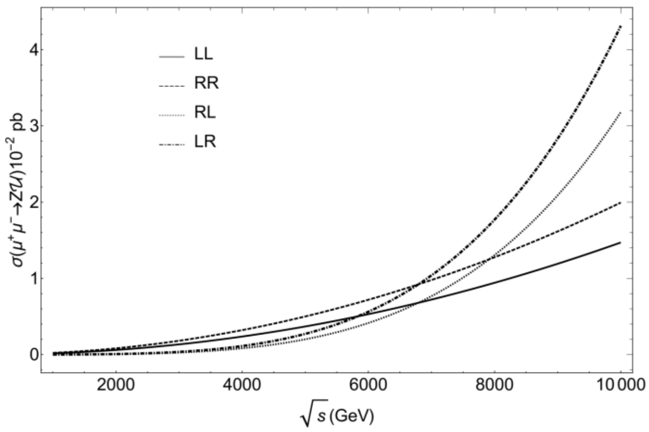

Figure 7. Total cross sections as functions of $\sqrt{s}$ for the process $\mu^+\mu^- \to ZU$ through u-channel.

In this part, we concentrate on total cross sections versus $\sqrt{s}$ in the appropriate energy range. The energy reach we consider in the article is possible at the present and future energy frontiers muon colliders, namely 4 TeV muon collider FNAL at Fermilab, a pulsed 14 TeV $\mu^+\mu^-$ collider in the LHC tunnel at CERN [14, 6] to the U.S. Muon Accelerator Program (MAP) colliders in the scheme [15]. Due to the neutrino radiation, the ultimate colliding-beam energy is limited at the ground level, as for the present designing assumptions, it constrains the center-of-mass energy to below 10 TeV. In Figure 6, the total cross sections in s-channel decline considerably as $\sqrt{s}$ raising to 3 TeV, and more gradually when $\sqrt{s}$ above 3 TeV region. The *RR* is about 1.3 times greater than *LL* , as can be seen in Figure 11. The total cross sections increase for each different $\mu^+\mu^-$ beams as $\sqrt{s}$ from 1 to 10 TeV (Figure 7).

The *LR* and *RL* reach the peak at 4.3×10^{-2} and 3.17×10^{-2} pb when $\sqrt{s}$ stands at 10 TeV, while the cross sections of *RR* and *LL* are going up more deliberately in the 4-6 TeV region. Overall, at the high energy from 8 to 10 TeV, total cross sections of *RL* and *LR* are increasing greater than *LL* and *RR*. We will evidently have more chances of observing the existence of the unparticle when the incoming beams are differently polarized.

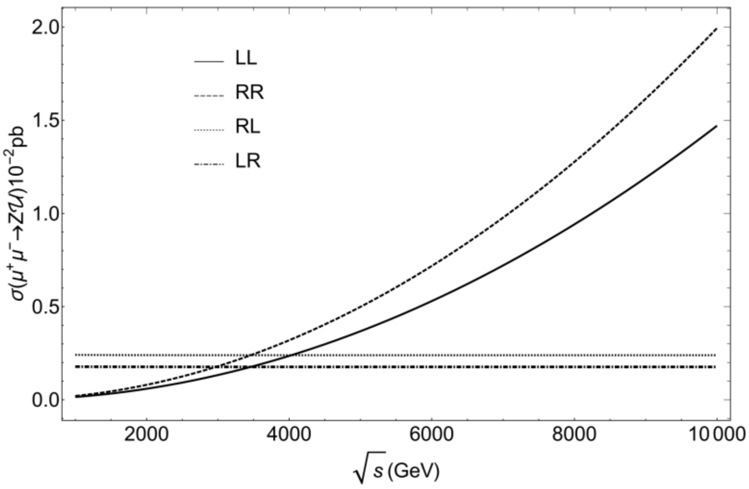

Figure 8. Total cross sections as functions of $\sqrt{s}$ for the process $\mu^+\mu^- \to ZU$ through t-channel.

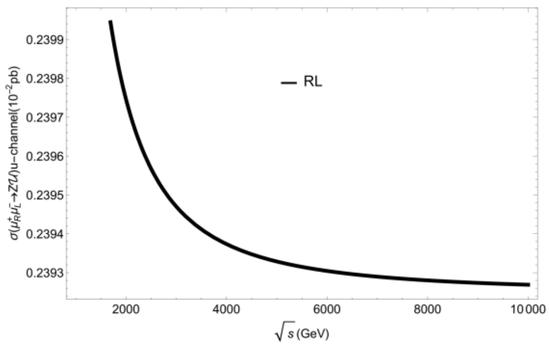

(a) RL

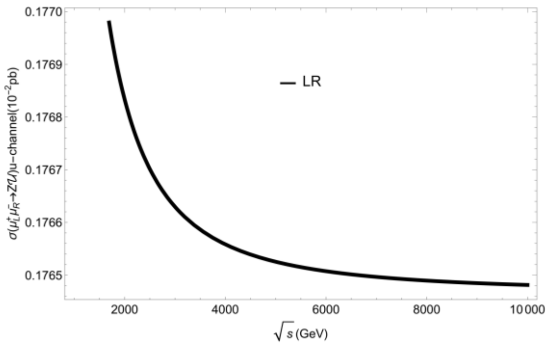

(b) LR

Figure 9. Total cross sections as functions of $\sqrt{s}$ for the *RL* and *LR* beams.

Through t-channel (Figure 8), the total cross sections of *RR* and *LL* have the maximum values of 2×10^{-2} to 1.47×10^{-2} pb with $\sqrt{s}$ at 10 TeV, they soars when $\sqrt{s}$ gradually rises from 6 to 10 TeV. In contrast, the *RL* and *LR* cross sections are trivial and remaining at around 0.24×10^{-2} pb and 0.177×10^{-2} pb in the region beyond 2 TeV. In Figure 9, we see the dive in the energy at above 2 TeV.

The numerical result indicates that the *RR* and *LL* beams lose their energy through mainly t-channel, which is contrary to the u-channel as the Figure 7 shown before. Through three different channels, the total cross sections of the *RL* and *LR* beams are the largest in u-channel. From theoretical perspectives, the existence of the scalar unparticle is observed along with the loss of energy of the initial $\mu^+\mu^-$ beams. As such, we could find out from these results that at the high energy region from 8 to 10 TeV, the losses of energy will be likely to happen through all the channels attributed to the unparticle as we expect, the polarized conditions of the initial beams *RL* and *LR* contributed the most (in Figure 7, 8).

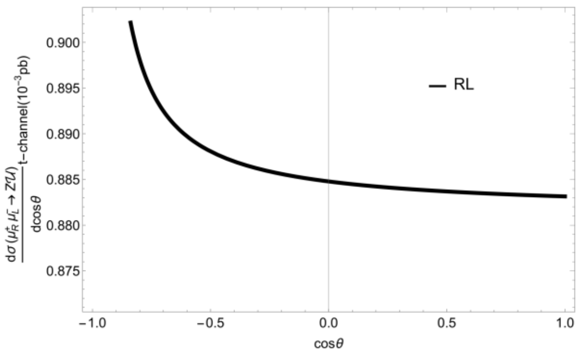

(a) RL

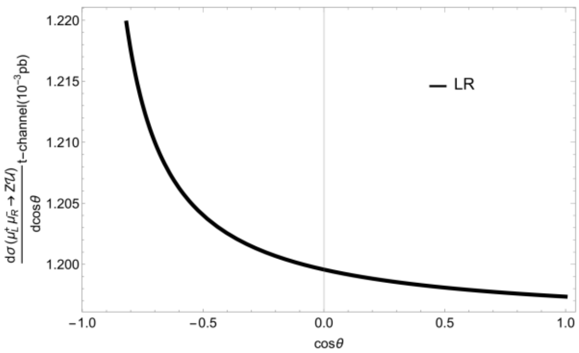

(b) LR

Figure 10. Differential cross sections as functions of $\cos\theta$ in u-channel for the *RL* and *LR* beams at 3 TeV.

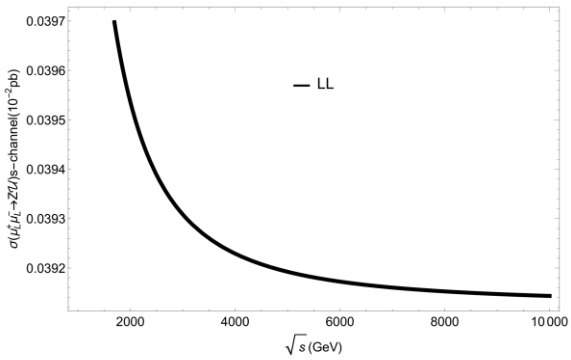

(a) RL

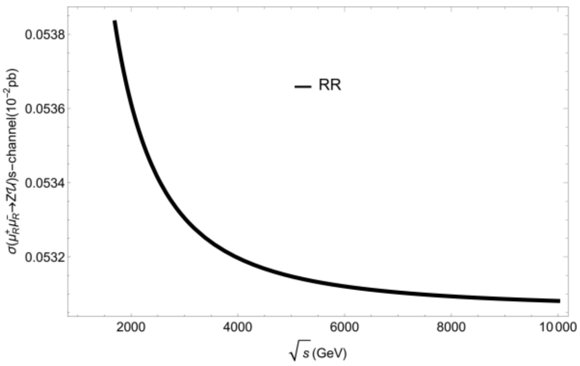

(b) LR

Figure 11. Total cross sections as functions of $\sqrt{s}$ for the process $\mu^+\mu^- \to ZU$ through s-channel for the *LL* and *RR* beams.

4. Conclusion

In the preceding sections, we have done primary mathematical calculations and plotted the cross sections as functions of the scattering angle and the collision energy. As for the scattering angle, it is found out that the advantageous direction of investigating the scalar unparticle signal is that the $\mu^+\mu^-$ beams and final production *U* are perpendicular to each other in u- and t-channel with the collision energy at 3 TeV. The results for total cross sections show that the possibility of the existence of scalar unparticle in experiments is high when polarized conditions of the $\mu^+\mu^-$ beams are *LR* and *RL* in u-channel when the collision energy is over 8 TeV. As a whole, we would still have many technical obstacles to overcome, the future high energy frontiers muon colliders are hoped to detect and measure precisely the existence and influence of the scalar unparticle at the collisions.

References

[1] T. Banks, A. Zaks, On the phase structure of vector-like gauge theories with massless fermions, Nucl. Phys. B196 (1982) 189–204.

[2] H. Georgi, Unparticle physics, Phys. Rev. Lett. 98 (2007) 221601. https://doi.org/10.1103/physrevlett.98.221601

[3] V. Khachatryan, A.M. Sirunyan, A. Tumasyan, W. Adam, E. Asilar, T. Bergauer, J. Brandstetter, E. Brondolin, M. Dragicevic et al., Search for dark matter and unparticles produced in association with a z boson in proton-proton collisions at ps = 8 tev, Phys. Rev. D 93 (2016) 052011. https://doi.org/10.1103/PhysRevD.93.052011.

[4] V. Khachatryan, A.M. Sirunyan, A. Tumasyan, W. Adam, T. Bergauer, M. Dragicevic, J. Erö, C. Fabjan, M. Friedl, R. Frühwirth, and et al., Search for dark matter, extra dimensions, and unparticles in monojet events in proton–proton collisions at ps = 8 tev, Eur. Phys. J. C 75 (5). https://doi.org/10.1140/epjc/s10052-015-3451-4.

[5] A.M. Sirunyan, A. Tumasyan, W. Adam, E. Asilar, T. Bergauer, J. Brandstetter, and E. Brondolin, M. Dragicevic, J. Erö et al., Search for dark matter and unparticles in events with a Z boson and missing transverse momentum in proton-proton collisions at ps = 13 tev, Journal of High Energy Physics 3. https://doi.org/10.1007/JHEP03(2017)061.

[6] V.D. Shiltsev, High-energy particle colliders: past 20 years, next 20 years, and beyond, Physics-Uspekhi 55 (10) (2012) 965–976. https://doi.org/10.3367/ufne.0182.201210d.1033.

[7] F. Zimmermann, High-energy physics strategies and future large-scale projects, Nuclear Instruments and Methods in Physics Research Section B: Beam Interactions with Materials and Atoms 355 (2015) 4 – 10, Proceedings of the 6th International Conference Channeling:"Charged and Neutral Particles Channeling Phenomena" October 5-10, 2014, Capri, Italy. https://doi.org/10.1016/j.nimb.2015.03.090.

[8] F. Zimmermann, Future colliders for particle physics —"big and small", Nucl. Instrum. Meth. A909 (2018) 33–37. https://doi.org/10.1016/j.nima.2018.01.034.

[9] The $\mu^+\mu^-$ Collaboration, $\mu^+\mu^-$ Collider: A Feasibility Study, BNL-52503, Fermi Lab-Conf. 96/092, LBNL-38946, Snowmass, 1996, Ch. 1. Introduction and Overview, pp. 2–4.

[10] S. Coleman, E. Weinberg, Radiative corrections as the origin of spontaneous symmetry breaking, Phys. Rev. D 7 (1973) 1888–1910. https://doi.org/10.1103/PhysRevD.7.1888.

[11] K. Cheung, W.-Y. Keung, T.-C. Yuan, Collider phenomenology of unparticle physics, Phys. Rev. D 76 (2007) 055003. https://doi.org/10.1103/PhysRevD.76.055003.

[12] S.-L. Chen, X.-G. He, Interactions of unparticles with standard model particles, Phys. Rev. D 76 (2007) 091702. https://doi.org/10.1103/PhysRevD.76.091702.

[13] M.E. Peskin, D.V. Schroeder, An Introduction to Quantum Field Theory, Addision-Wesley Publishing, 2018.

[14] D. Neuffer, V. Shiltsev, On the feasibility of a pulsed 14 TeV c.m.e. muon collider in the LHC tunnel, Journal of Instrumentation 13 (10) (2018) T10003–T10003. https://doi.org/10.1088/1748-0221/13/10/t10003.

[15] J.-P. Delahaye, C. Ankenbrandt, A. Bogacz, S. Brice, A. Bross, D. Denisov, E. Eichten, P. Huber, D. M. Kaplan, H. Kirk, R. Lipton, D. Neuffer, M.A. Palmer, R. Palmer, R. Ryne, P. Snopok, Enabling intensity and energy frontier science with a muon accelerator facility in the united states: A white paper submitted to the 2013 united states community summer study of the division of particles and felds of the american physical society (2013). arXiv:1308.0494.